International Journal of Air-Conditioning and Refrigeration Vol. 16, No. 4 (2008) 124~129

Determination of an Optimum Orbiting Radius for an Oil-Less Scroll Air Compressor

Hyun Jin Kim †, Yong Ho Lee*, Tae Hun Kwon*

Department of Mechanical Engineering, University of Incheon, Incheon 402-749, Korea
**Department of Mechanical Engineering, Graduate school, University of Incheon, Incheon 402-749, Korea*

(Received October 22, 2008; Revision received December 10, 2008; Accepted December 18, 2008)

Abstract

Design practice has been made on an oil-less scroll air compressor as an air supply device for a 2 kW fuel cell system where air pressure of 2 bar and flow rate of 120 liter/min are required. Basic structure of the scroll compressor includes double-sided scroll wrap for the orbiting scroll driven by two crankshafts connected to each other by a timing belt. These features can eliminate thrust surface which otherwise would produce frictional heat and jeopardize reliable operation of the orbiting scroll and the scroll element's deformation as well. This study focuses on optimum scroll wrap design; orbiting radius has been chosen as an independent design parameter. As the orbiting radius changes, scroll sizes such as scroll base plate and discharge port diameters change accordingly. Gas compression-related losses and mechanical loss also change with the orbiting radius. With a scroll base plate diameter of 120mm at most and discharge port of at least 10mm, the orbiting radius should be within the range of 2.5-4.0mm. With this range of the orbiting radius, it was estimated by performance analysis that the compressor efficiency reached to a maximum of $\eta_c = 96\%$ at the orbiting radius of $r_s = 3.5$mm for the scroll wrap height-to-thickness ratio of h/t=5.

Key words: Scroll compressor, Orbiting radius, Wrap design, Efficiency

Nomenclature

F : Force [N]
h : Wrap height [m]
L : Loss [W]
l : Length [m]
l_p : Length from Orbiting scroll center to Crankshaft eccentric center [m]
m_{os} : Mass of Orbiting scroll [kg]
$\dot{m}_{os}$: mass flow rate [kg/s]
N : Shaft speed [rpm]
P : Pressure [bar]
P_e : Stack power [kW]
Q_s : Flow rate [lpm]
r_s : Orbiting radius [m]
t : Wrap thickness [m]
t_s : Suction temperature [?C]
V : Volume [cc]
V_c : Voltage of each cell in the stack [V]
$V.R$: Volume ratio
W_c : Compressor input [W]

Greek symbols

α : Starting angle [°]
ϕ : Involute angle [°]
η : Efficiency [%]
λ : Stoichiometric coefficient
μ : Friction coefficient
θ : Crank angle [°]
ω : Angular velocity [rad/s]

†Corresponding author. Tel.: +82 32 770 8419, Fax.: +82 32 770 8423
E-mail address: kimhj@incheon.ac.kr

1. Introduction

As the air compressor consumes the most electric power among the peripheral devices of a fuel cell, increasing the efficiency of the air compressor is essential to improve the overall efficiency of the fuel cell system. A turbo-type air compressor is adequate for a large capacity generator since it requires a significant amount of air supply, and a positive displacement air compressor is more suitable for a small

or medium capacity system.

The rotary vane type has mainly been used as the positive displacement air compressor for fuel cell applications.

A typical rotary vane air compressor involves a vane rotating by the centrifugal force while it is attached to the cylinder wall, creating substantial friction loss between the vane hem and the cylinder wall, and generating an excessive amount of heat. Several means of resolving these problems have been suggested[1,3], but significant improvements have not yet been reported.

A scroll type compressor has a fundamentally different structure than the rotary vane type. In a scroll compressor, the crankshaft rotates 2-3 times from intake to outlet, which yields smooth compression and little variation of torque to facilitate a less noisy operation. Thanks to the scroll compressor's highly efficient characteristics, low noise and low vibration, oil-less scroll air compressors have been introduced for general industrial purposes, but their compressor ratios are 7 or greater, making them inadequate for fuel cell applications, which require low-pressure air.

Based on the basic structure of the oil-less scroll air compressor for industrial applications, this study proposes an approach for designing a scroll air compressor applicable to the fuel cell system and suggests the estimated size and performance of the scroll air compressor for fuel cell applications under given conditions regarding its capacity and operation.

2. Conceptual design

2.1 Basic structure of scroll air compressor

Air compressor for fuel cell application should deliver pure air, particularly free of oil containment, and it should also be a highly reliable for long periods of continuous operation. Since oil is essential to compressors in terms of cooling and lubrication, oil-less operations for fuel cell air compressors demand many particular requirements such as special surface treatment on the sliding parts of the compressor and some design techniques such as design of avoiding sliding surfaces as much as possible and of reducing frictional heat generation. Considering these aspects, a schematic of the basic structure of a scroll air compressor is presented in Fig. 1.

For the double-sided scroll wrap structure, the axial gas forces action on both sides of the orbiting scroll plate to balance each other so that no thrust surface is

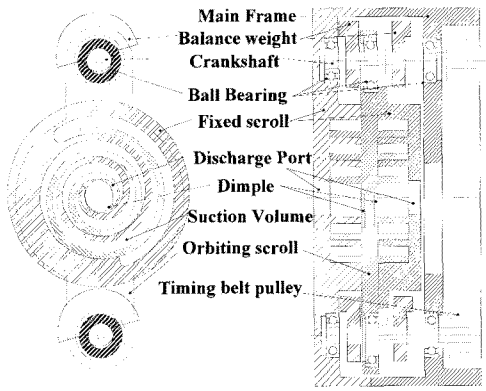

Fig. 1. Basic structure of scroll air compressor.

Table 1. Scroll configuration factors.

Configuration factors		Relations
symbols	Description	
a	Base circle radius	$r_s = a\pi - t$ $t = 2a\alpha$ $V_s = 2\alpha a r_s h(2\phi_e - 3\pi)$ $V.R = \frac{2\phi_e - 3\pi}{2\phi_a + \pi}$
t	Wrap thickness	
h	Wrap height	
r_s	Orbiting radius	
ϕ_e	Wrap end angle	
ϕ_a	Cutter angle	
α	Starting angle	
7 parameters		4 equations

required and generation of frictional heat is completely eliminated. In refrigerating scroll compressors, Oldham coupling is used to make the orbiting scroll orbit instead of self-rotate. In such a device, Oldham ring keys are inserted into key slots provided on the rear of the orbiting scroll base plate and lubricating oil needs to be applied to the sliding surfaces between the keys and the key slots. For fuel cell application, air free of oil should be applied to the cathode of the fuel cell, such lubricating oil cannot be applied. Instead of using an Oldham coupling device for the present configuration, two crankshafts are inserted into the two hubs located on either of the orbiting scroll base plate, and these two crankshafts are connected to each other by a timing belt so that the crankshafts can function as anti-rotation devices for the orbiting scroll. Driving power from motor is transmitted to one of the crankshafts.

To reduce leakage through the wrap tip clearance of the neighboring compression pockets, tip seal is applied to the wrap top surface. Sliding bush used for reducing flank leakage in scroll compressors is not considered here for simplicity.

2.2 Scroll wrap configuration factors

There are 7 scroll wrap configuration factors as in Table 1 and 4 relations among them can be obtained.

The wrap height is limited compared to the wrap thickness because gas force exerted on the wrap side could cause some degree of deflection and some difficulty could be encountered in machining scroll wrap with large aspect ratio. For fuel cell application, relatively low-pressure air is required, so that the effect of the gas force exerted on the wrap side may be negligible. So the wrap height limitation could come from the manufacturing consideration. In the present design, aspect ratio of the wrap of h/t=5 will be chosen. Also a wrap thickness of t=3.7mm will be used. This is nearly the minimum thickness for tip seal installation.

With this determination of the wrap thickness and the aspect ratio of the wrap, it can be regarded that the number of unknown parameters was reduced from 7 to 6, and that one more relation among the parameters was added to the existing 4 relations in Table 1. Therefore, since there are 6 unknowns with 5 relations among them, only one parameter can be selected as an independent parameter. In this study, the orbiting radius will be chosen as an independent one, since it has a direct influence on the compressor performance.

Since built-in volume ratio $V.R$ is related to the design pressure ratio as in equation (1), and displacement volume V_s is related to the design flow rate Q_s as in equation (2), these two, $V.R$ and V_s, can be determined by operating conditions at the design point.

$$V.R = V_s / V_d = (P_d / P_s)^{1/n} \quad (1)$$

$$Q_s = \eta_v V_s N / 60 \quad (2)$$

2.3 Design conditions

To design a scroll compressor that supplies air to the fuel cell of 2 kW power output, required air-flow rate can be estimated by equation (3).[4]

$$\dot{m}_s = 3.57\times10^{-7}\times\lambda\times\frac{P_c}{V_c}\ [\mathrm{kg/s}] \quad (3)$$

For stoichiometry of $\lambda = 2$, and stack voltage of $V_c = 0.6V$, required air-flow rate $\dot{m}_s = 0.00238$ kg/s was calculated. This corresponds to the volume flow rate of $Q_s = 120$ lpm for the suction condition of 1 bar and 25℃. Operating conditions with required air-flow rate are summarized in Table 2.

Table 2. Design conditions.

Notation	Description	Values
Q_s	Flow rate	120 lpm
P_s	Suction pressure	1 bar
t_s	Suction temperature	25℃
P_d	Discharge	2 bar
N	Shaft speed	3500 rpm

Table 3. Combination of scroll configuration factors for displacement volume of 42.9cc.

r_s	a	α	ϕ_e	ϕ_a
2.5	1.814 mm	53.7°	1340°	562°
3	1.973 mm	49.7°	1095°	412°
3.5	2.132 mm	46.3°	928°	311°
4	2.291 mm	43.3°	808°	237°

Assuming volumetric efficiency of $\eta_v = 80\%$ for shaft speed $N = 3500$ rpm, displacement volume is determined to be $V_s = 42.9$ cc from equation (2). From design pressure ratio of 2, built-in volume ratio is obtained to be $V.R = 1.6407$ by equation (1).

2.4 Effects of orbiting radius on scroll configuration

Fig. 2 shows variation of $a\phi_e$, corresponding to the distance from scroll center to the wrap end, and $a\phi_a$, an indication of discharge port size, and orbiting scroll mass, m_{os}, with the variation of the orbiting radius, r_s. With increasing r_s, the distance from scroll center to the wrap end and the discharge port size decrease. In the present design, an orbiting scroll base plate diameter not larger than 120mm and discharge port not smaller than 10mm are required, yielding to a range of the orbiting radius of

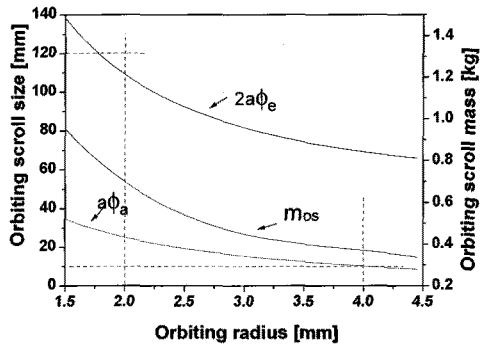

Fig. 2. Scroll size vs. orbiting radius.

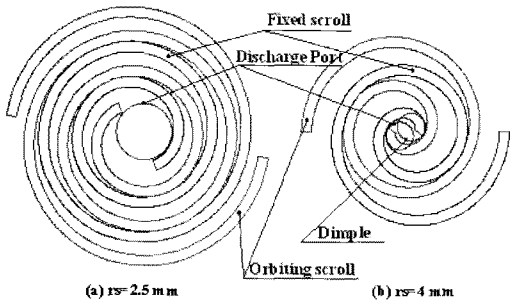

Fig. 3. Scroll wrap profiles.

$2.5\ \text{mm} < r_s < 4.0\ \text{mm}$. In Fig. 3, scroll profiles at the two extreme cases are shown.

3. Performance analysis and discussions

3.1 Volume diagram

Volume diagrams for various orbiting radius are shown in Fig. 4. As the orbiting radius increases, the decreasing rate of the compression chamber volume increases with an earlier start of discharge.

3.2 Pressure and gas force

Calculated P-V diagram is shown in Fig. 5. The pressure calculation was carried out by assuming polytropic compression, taking into account leakages among neighboring compression pockets.[2] Leakage clearance was assumed to be $20\mu m$ for both wrap tip and flank leakages. With increasing the orbiting radius, leakage loss decreases, but over-compression loss also increases. This is because the leakage length for the wrap tip decreases and discharge port diameter decreases with increasing the orbiting radius.

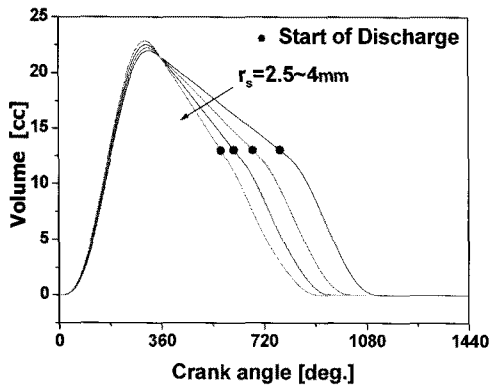

Fig. 4. Volume diagram

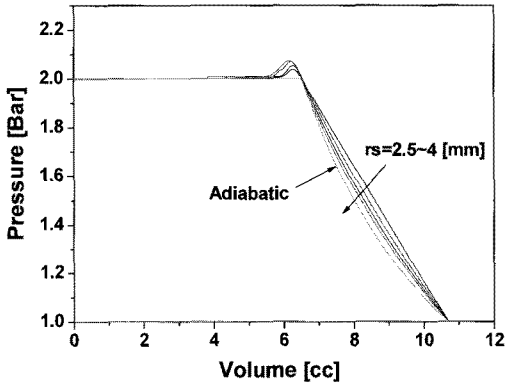

(a) A pocket

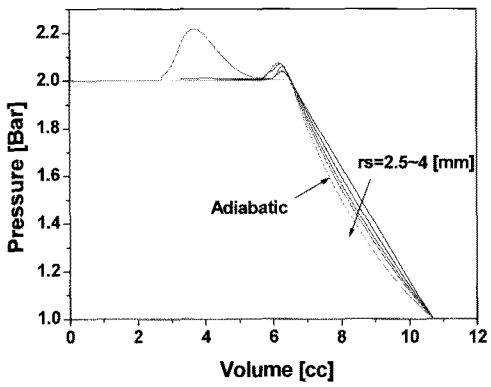

(b) B pocket

Fig. 5. P-V diagram.

Particularly at the orbiting radius of $r_s = 4.0$ mm , over-compression loss becomes larger in compression pocket B than in pocket A, since it is more difficult to secure enough passage for discharge for compression pocket B at this scroll configuration. As a whole, the gas compression loss appeared to be a minimum at $r_s = 3.5$ mm .

Fig. 6 shows gas forces acting on the orbiting scroll together with its centrifugal force. Tangential gas force F_{rg} decreases with increasing r_s . This is due to a smaller scroll size with a larger orbiting radius while the wrap height is held constant, as shown in Fig. 2. Radial gas force F_{rg} is smaller compared to F_{rg} , its magnitude being insensitive to the change of r_s . While the mass of the orbiting scroll becomes smaller with larger r_s as shown in Fig. 2, the centrifugal force F_{osc} increases slightly as a result of the product of the mass sand the orbiting radius.

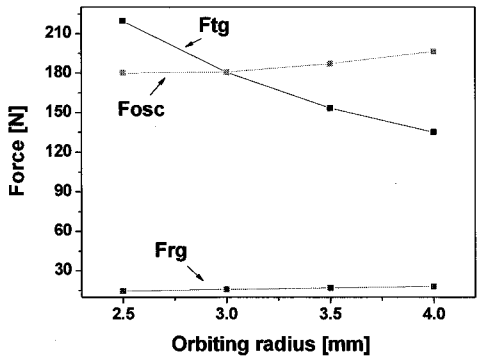

Fig. 6. Gas force.

3.3 Dynamics of moving elements

Fig. 7 and Fig. 8 show forces acting on the orbiting scroll and the crankshaft, respectively. From these force diagrams, equations of force and moment balances can be obtained as in equations (4)-(10).

$$F_{x1}+F_{x2}+2F_{tg}\sin\theta+(F_{osc}-2F_{rg})\cos\theta=0 \quad (4)$$

$$F_{y1}+F_{y2}+2F_{tg}\cos\theta-(F_{osc}-2F_{rg})\sin\theta=0 \quad (5)$$

$$F_{y1}l_p-F_{y2}l_p+r_sF_{tg}+r_{cp}\mu_{cp}F_{cp1}+r_{cp2}\mu_{cp}F_{cp2}=0 \quad (6)$$

$$-F_{ur}+\mu_{ub}F_{ut})-F_{dr}+\mu_{db}F_{dt}-F_{uwc}-F_{dwc}+F_{cpc}+F_{cpr}=0 \quad (7)$$

$$-(F_{ut}-\mu_{ub}F_{ur})-(F_{dt}-\mu_{db}F_{dr})+F_{cpt}=0 \quad (8)$$

$$(F_{ur}-\mu_{ub}F_{ut})l_{ub}+F_{uwc}l_{uw}-F_{dwc}l_{dw}-(F_{dr}-\mu_{db}F_{dt})l_{db}=0 \quad (9)$$

$$-(F_{ut}-\mu_{ub}F_{ur})l_{ub}+(F_{dt}-\mu_{db}F_{dr})l_{db}=0 \quad (10)$$

Resultants of force components at the two crankshaft eccentrics engaged with the corresponding orbiting scroll hubs, (F_{x1}, F_{y1}) and (F_{x2}, F_{y2}) can be written as $F_{cp1}=\sqrt{F_{x1}^2+F_{y1}^2}$ and $F_{cp2}=\sqrt{F_{x2}^2+F_{y2}^2}$, respectively. Also, shaft bearing loads at upper and lower supports are $F_{ub}=\sqrt{F_{ut}^2+F_{ur}^2}$ and $F_{db}=\sqrt{F_{dt}^2+F_{dr}^2}$, respectively.

Mechanical losses at all sliding surfaces are given by equation (11).

$$L_{mech}=2\omega(r_{cp}\mu_{cp}F_{cp}+r_{ub}\mu_{ub}F_{ub}+r_{db}\mu_{db}F_{db}) \quad (11)$$

Ball bearings were used for the crankshaft eccentrics and shaft supports. Friction coefficient of the ball bearing was 0.0015.

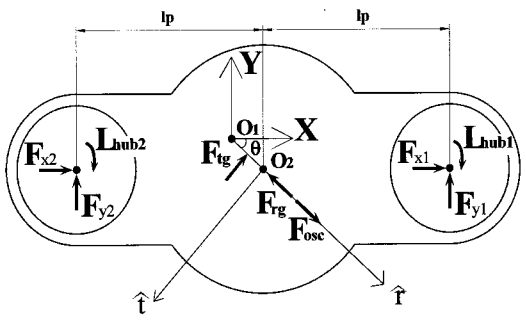

Fig. 7. Force diagram on orbiting scroll.

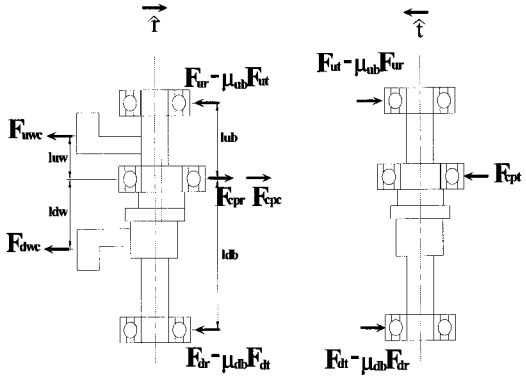

Fig. 8. Force diagram on crankshaft.

3.4 Calculation results

Calculated bearing forces at the crankshaft eccentrics and shaft supports are shown in Fig. 9. As the orbiting radius r_s increases, bearing forces decrease due to decreasing F_{tg} with increasing r_s.

For various values of the orbiting radius, compressor input power together with various compressor losses were summarized in Table 4. Adiabatic compression power to compress the ambient air to 2 bar at

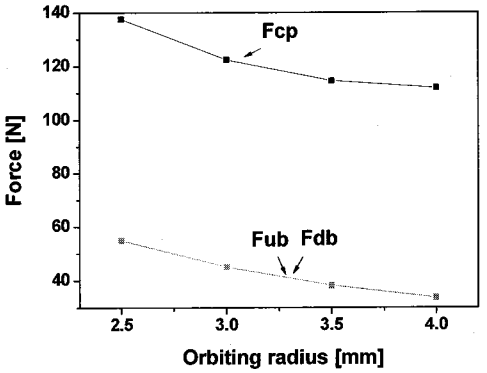

Fig. 9. Bearing loads.

Table 4. Calculation results of compressor input power and loss breakdown.

Loss \ r_s (mm)	2.5	3.0	3.5	4.0
L_{gas}(W)	9.44	7.54	5.15	7.7
L_{mech}(W)	2.86	2.47	2.24	2.11
W_c(W)	203.8	201.5	198.8	201.1

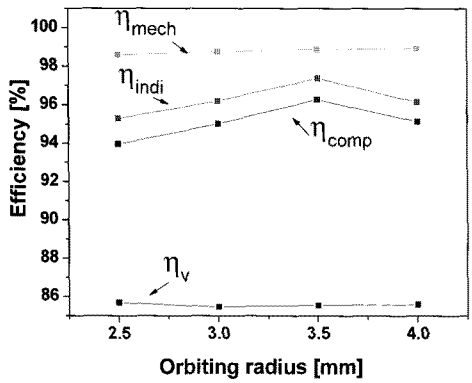

Fig. 10. Compressor efficiencies.

the flow rate of 120 lpm is 191.4 W.

Gas compression loss was calculated to be around 5W~9W, depending on r_s. Minimum gas compression loss was obtained at $r_s = 3.5$ mm.

Mechanical loss increased slightly with decreasing r_s in the range of 2W~3W. As a consequence, minimum compressor input power was obtained at $r_s = 3.5$ mm.

Fig. 10 shows various efficiencies of the compressor. As r_s increased, mechanical efficiency increased slightly from 98.59% to 98.94%. Indicated efficiency showed a maximum value of $\eta_{indi} = 97.38\%$ at $r_s = 3.5$ mm, resulting in a maximum of the total compressor efficiency as the product of the mechanical and indicated efficiencies at the same r_s. The maximum compressor efficiency was $\eta_{comp} = 96.28\%$. Volumetric efficiency of around 85.5% did not change much with r_s.

4. Conclusions

In an analytical study on the applicability of scroll type compressor to oil-less air compressor used for the fuel cell systems,

(1) Conceptual design has been carried out to supply air of 2 bar to 2 kW fuel cell system: Designed scroll compressor is characterized by a double-sided orbiting scroll driven by two crankshafts, which also function as anti-rotation devices.

(2) Orbiting radius was selected as an independent variable among 7 scroll wrap configuration factors. As the orbiting radius increased, the diameters of the scroll base plate and discharge port decreased: In order to design the base plate smaller than 120mm and the discharge port larger than 10mm, the orbiting radius needs to be in the range of $2.5 \text{ mm} < r_s < 4.0 \text{ mm}$.

(3) As the orbiting radius increased from 2.5mm to 4.0mm, the mechanical efficiency increased slightly from 98.59% to 98.94%, and the indicated efficiency showed a maximum of 97.38% at $r_s = 3.5$ mm, resulting in a maximum compressor efficiency of 96.28% at the same orbiting radius. Volumetric efficiency was about constant at 85.5%, regardless of r_s.

References

[1] Drive, R.W., Davidson, D.P., 1999, Applications for the hinge-vane positive displacement compressor-expander, International Conference on Compressors and Their Systems, Institution of Mechanical Engineers, London, pp.339-348.

[2] Kim, H.J., Kim, J.H., Lee, J.K., 1998, Dynamic behavior of a scroll compressor with radial compliant device, Korean Journal of Air-Conditioning and Refrigeration Engineering, Vol. 10, No.1, pp.33-43.

[3] Kim, H.Y., Lee, Y.H., Kim, H.J., Joo, B.S., 2007, A study on the friction loss reduction in a rotary vane air compressor, Proceedings of SAREK 2007 Summer Annual Conference, Paper No. 07-S-002.

[4] Larminie, J., Dicks, A., 2003, Fuel Cell Systems Explained, Wiley, Hoboken